



# ISAT v2.0: an integrated tool for nested-domain configurations and model-ready emission inventories for WRF-AQM

Kun Wang<sup>1,6</sup>, Chao Gao<sup>2</sup>, Kai Wu<sup>3</sup>, Kaiyun Liu<sup>4</sup>, Haofan Wang<sup>5</sup>, Mo Dan<sup>1</sup>, Xiaohui Ji<sup>1</sup>, and Qingqing Tong<sup>2</sup>

<sup>1</sup>Institute of Urban Safety and Environmental Science, Beijing Academy of Science and Technology, Beijing 100054, China

<sup>2</sup>Key Laboratory of Wetland Ecology and Environment, Northeast Institute of Geography and Agroecology, Chinese Academy of Sciences, Changchun 130102, China

<sup>3</sup>Department of Civil and Environmental Engineering, University of California, Irvine, CA 92697, USA

<sup>4</sup>State Key Joint Laboratory of Environment Simulation and Pollution Control, School of Environment, Tsinghua University, Beijing 100084, China

<sup>5</sup>School of Atmospheric Sciences, Sun Yat-sen University, Zhuhai, Guangdong, China

<sup>6</sup>Key Laboratory of Marine Environmental Science and Ecology, Ministry of Education, Ocean University of China, Qingdao 266100, China

**Correspondence:** Kaiyun Liu (liuky2021@tsinghua.edu.cn) and Xiaohui Ji (jixiaohui@bmlp.com)

Received: 3 November 2022 – Discussion started: 3 January 2023

Revised: 10 March 2023 – Accepted: 14 March 2023 – Published: 6 April 2023

**Abstract.** The ISAT (Inventory Spatial Allocation Tool) v2.0 is an integrated tool that has been developed to configure nested domains, downscale regional emission inventories, allocate local emission inventories, and generate model-ready emission inventories for the Weather Research and Forecasting (WRF)–Air Quality Numerical Model (AQM). The tool consists of four modules, namely “Prepgrid”, “Downscale”, “Mapinv”, and “Prepmodel”, which are designed to perform specific tasks. The Prepgrid module utilizes a nested-domain configuration algorithm based on WRF-AQM nested rules and the target domain shapefile. The Downscale module establishes a “sub-grid nearest” method to downscale the regional emission inventory based on spatial surrogate, thereby improving the accuracy and computational efficiency of the process. The Mapinv module allocates a user-defined regional- and/or city-level emission inventory to grid level based on the target domain shapefile and the spatial surrogate. Finally, the Prepmodel module generates the model-ready inventories by introducing unique user-friendly emission sector IDs using abbreviations and speciation profiles based on species in the emission inventory and chemical mechanisms, which is available for both the CMAQ and CAMx models. The ISAT v2.0 tool provides a user-friendly solution for model users to configure and run WRF-AQM.

And it provides a framework and related algorithms for researchers to develop similar tools for WRF-AQM.

## 1 Introduction

High-spatial- and temporal-resolution emission inventories (HREIs) of air pollutants are essential for atmospheric environmental mitigation strategies, ambient air quality forecasting, and research on air pollution, as they can quantify pollutant concentrations based on an air quality model (AQM), such as the Weather Research and Forecast (WRF)–Community Multiscale Air Quality (CMAQ) model (Burnett et al., 2018; H. Wang et al., 2022; K. Wang et al., 2022a). Preparing HREIs requires spatial allocation, temporal allocation, and chemical speciation. Spatial allocation maps areas and point emissions into the AQM domain based on source locations and spatial surrogates (Z. Huang et al., 2021; Zheng et al., 2021; Zhou et al., 2017). Temporal allocation provides hourly emissions based on temporal profiles, such as monthly production statistics, heating degree days, and temporal variation in traffic activity (K. Wang et al., 2021a). Chemical speciation produces speciated emissions for specific mechanisms, such as CB05 or SAPRC99, based on speciation pro-

files that provide the composition of organic gases and particulate matter in sectors (Huang et al., 2015).

The downscaling of regional emission inventory (REI) disaggregated atmospheric emissions from a national or regional scale to the grid level provides a method for obtaining an HREI for an AQM, such as the MEIC, with a spatial resolution of  $0.25^\circ$  (ECJRC, 2017; Li et al., 2017; Zheng et al., 2018). The process involves using a spatial surrogate to represent a fraction of the total national and regional emissions on a target grid between zero and 1 (Eyth and Hanisak, 2003). Proxies such as population density, land use, and road maps were developed as spatial surrogates for the intensity of real activity in residential, agriculture, transportation, and other sectors (Lin et al., 2022; Wang et al., 2017). The nearest method is a popular downscaling method, which locates the closet REI value on the target grid and allocates emissions using spatial surrogates (Zhang et al., 2014; Zhuang et al., 2022). However, the use of this method may amplify the emission mismatch without considering a projection difference that may exist between the AQM and the REI, which may be caused by the changes in the research domain. The intersect method splits the target domain into several parts between the target domain and the REI, which accounts for the projection difference but may lead to low calculation efficiency. Therefore, a new algorithm is necessary to improve both calculation efficiency and accuracy in the REI downscaling process.

Various emission inventory processing tools have been previously developed, yet an integrated tool for domain configuration to model-ready inventory workflow for WRF-AQM is unavailable. For example, TEMMS can only support the emission of transportation (Namdeo et al., 2002), and THOSCAN cannot create a model-ready emission inventory for AQMs (Monforti and Pederzoli, 2005). SMOKE, a Linux-platform-supported and widely used tool in AQMs, requires a predefined spatial surrogate from other geoprocessing tools, such as ArcGIS, and cannot define parameters for nested domains in WRF-AQM (Baek and Seppanen, 2021). The WRF Domain Wizard (<https://esrl.noaa.gov/gsd/wrfportal/DomainWizard.html>, last access: 30 March 2023) allows the user to configure nested domains by manually delimiting research areas. However, without the shapefile of the target area, obtaining precise domains is challenging, which requires several trials and expert experience to obtain suitable nested domains in AQMs. Therefore, it is essential to develop an integrated tool that ensures domain consistency and provides a user-friendly workflow from a nested-domain configuration to the WRF-AQM system.

Innovatively, a user-friendly and integrated tool, ISAT (Inventory Spatial Allocation Tool) v2.0, was developed from the nested-domain configuration to a model-ready emission inventory for WRF-AQM in this study. We established a nested-domain configuration algorithm based on a shapefile that ensures domain consistency between the WRF, AQM, and emission inventory. We proposed a regional inventory

downscaling algorithm called the “sub-grid nearest” method, which improved the computational efficiency and accuracy of the REI downscaling. We provided interfaces for a model-ready emission inventory for CMAQ and CAMx models. In addition, we embedded population- and road-based spatial surrogate data into the ISAT, which supports most spatial allocation workflows for WRF-AQM in China.

## 2 Materials and methods

We developed an integrated tool to complete the workflow from a nested-domain configuration to a model-ready HREI for WRF-AQM, as depicted in Fig. 1. The shapefiles provide location and extent in each domain used to configure nested domains in WRF-AQM by the Prepgrid module. For domains without a local emission inventory, REIs such as the MEIC can be downscaled into domains by the Downscale module. Local emission inventories can be allocated into domains by the Mapinv module. Both the CMAQ and CAMx models support inline plume rise calculations and inline-format HREI (Guevara et al., 2014). Based on gridded emissions from Downscale and Mapinv, the inline-format HREI for WRF-AQM can be created in Prepmodel. Users can adopt each module individually or in combination according to their needs. The methodological innovations in this study included a nested-domain configuration algorithm, a sub-grid nearest method, a user-friendly emission source ID, and speciation profiles, as detailed in the following sections.

### 2.1 Nested-domain configuration in Prepgrid

Using Arakawa C-grid staggering in the WRF model, a 3 : 1 grid-distance nesting ratio between domains is required for a nested-domain configuration (Skamarock et al., 2019). Nested domains can be classified into parent and child domains and initially configured based on the extent of shapefiles (Daniels et al., 2016). The outermost domain determines the projection in WRF-AQM. The child domains need to be extended based on user needs and the 3 : 1 grid-distance nesting ratio between domains. Users can set the number of extended grids in the east, west, south, and north directions as needed: ( $\text{add}_e$ ,  $\text{add}_w$ ,  $\text{add}_s$ , and  $\text{add}_n$ ). The number of grids that must be expanded under grid-distance nesting rules were also considered: ( $\text{add}_x$  and  $\text{add}_y$ ). Taking the  $x$  direction as an example,  $\text{add}_e$ ,  $\text{add}_w$ , and  $\text{add}_x$  were used to extend the domain in the WRF model, as shown in Fig. 2. Moreover, due to the outermost cells in WRF being inappropriate for use in an AQM (US EPA, 2019), *model\_clip* was conducted to define a lateral boundary for the AQM, as shown in Appendix A. In practice, we usually obtain the extent of the study area based on its shapefile. Compared with manual configuration, using a shapefile can provide a consistent and accurate nested do-

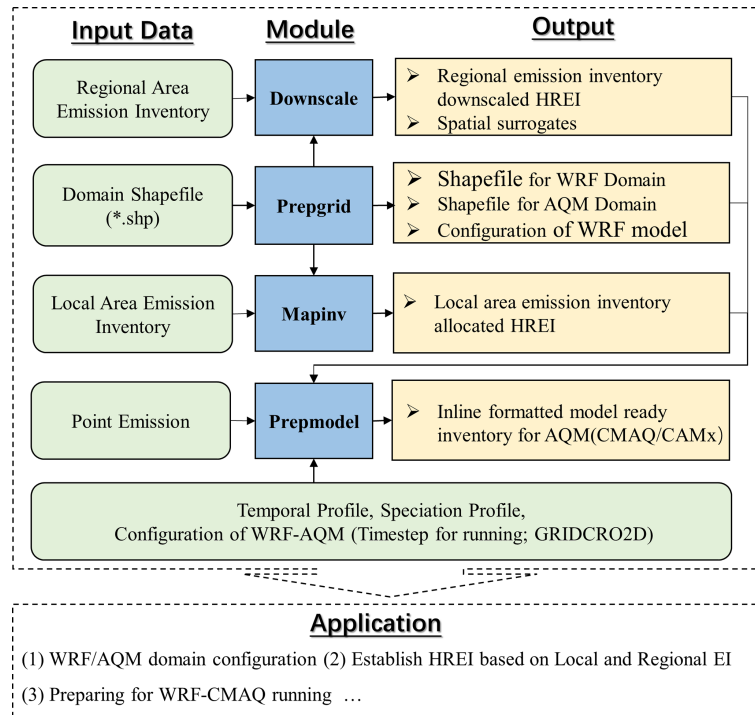


Figure 1. ISAT framework.

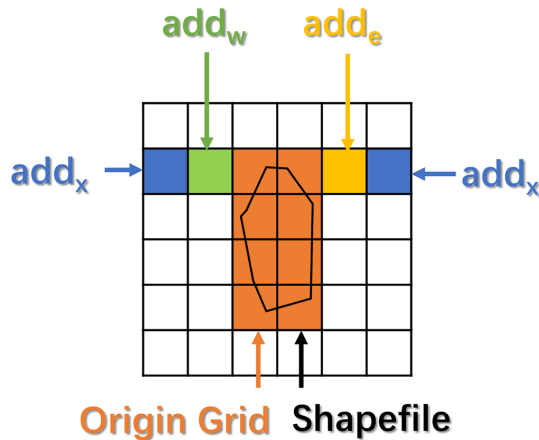


Figure 2. Parameters for modifying the domain in the  $x$  direction.

main between WRF, AQM, and an emission inventory. The major steps and key parameters are described below.

### 2.1.1 Projection configuration based on the outermost domain

Standard parallels, the central meridian, and the latitude of the Lambert conformal conic (LCC) projection can be obtained from the shapefile in the outermost domain. Due to defined grid spacing, the WRF-AQM domain may exceed the study area's shapefile; thus, the shapefile center does not rep-

resent the center of the LCC projection. We designed four main steps to accomplish projection configuration. (i) The first is setting standard parallels. Standard parallels were defined by users according to the location of the outermost domain (for example, Shanxi province configured with 33 and 42°). (ii) The second is setting the extent and number of grids in domain. Under the LCC projection in the previous step and the shapefile, we obtained the number of grids ( $num_x$  and  $num_y$ ) and origin ( $X_{min}$  and  $Y_{min}$ ) as shown in Eqs. (1)–(4). (iii) The third is updating LCC projection. The center of the domain was transferred into WGS 84 projection and used to update the center in LCC projection. (iv) The fourth is getting final LCC projection parameters, looped through steps (iii)–(ii)–(iii) until the difference in the center of the domain and shapefile in the loops could be ignored.

$$num_x = \text{Roundup} \left( \frac{disx}{dx} \right) + add_e + add_w, \quad (1)$$

$$num_y = \text{Roundup} \left( \frac{disy}{dy} \right) + add_s + add_n, \quad (2)$$

$$X_{min} = \frac{-(num_x \times dx)}{2}, \quad (3)$$

$$Y_{min} = \frac{-(num_y \times dy)}{2}, \quad (4)$$

where  $disx$  and  $disy$  represent the length of the shapefile in the  $x$  and  $y$  directions.

### 2.1.2 Determination of child domain parameters

Constrained by grid-distance nesting rules and lateral boundaries for the AQM, the child domain configuration step is different from the parent domain step. Spatial resolution and origin in the parent and child domains ( $dx_{par}$ ,  $dx_{child}$ ,  $xstart_{child}$ , and  $xstart_{parent}$ ) were adopted for the child domain configuration. Taking the  $x$  direction as an example, the number of grids was calculated based on the spatial coverage of the shapefile, user-defined parameters, and the number of grids constrained by the nesting rules in the WRF model, as shown in Eq. (5). The term  $add_x$  is the must-add number of grids according to the nesting rules and the shapefile in the parent and child domain, as shown in Eq. (6), and  $num_x$  was further corrected by Eqs. (7)–(8).  $X_{min}$  is the present start position of the child domain with a projection configuration based on the nesting rules and the user-defined  $add_w$  as shown in Eq. (9). Moreover,  $start_x$  denotes the starting position for the child domain in the parent domain, which can be used to configure a nested domain in the WRF model in Eq. (10).

$$num_{x,tmp} = \text{Roundup}\left(\frac{disx_{child}}{dx_{child}}\right) + add_e + add_w + add_x \quad (5)$$

$add_x =$

$$\text{Roundup}\left(\frac{xstart_{child} - \text{int}\left(\frac{xstart_{child} - xstart_{parent}}{dx_{par}}\right) \times dx_{par} - xstart_{parent}}{dx_{child}}\right) \quad (6)$$

$$tmpgrid_x = \text{mod}\left(num_{x,tmp}, \frac{dx_{par}}{dx_{child}}\right) \quad (7)$$

$$num_x = \begin{cases} num_{x,tmp} & (tmpgrid_x = 0) \\ num_{x,tmp} + \frac{dx_{par}}{dx_{child}} - tmpgrid_x & (tmpgrid_x \neq 0) \end{cases} \quad (8)$$

$$X_{min} = \text{integer}\left(\frac{xstart_{child} - xstart_{parent}}{dx_{par}}\right) \times dx_{par} + xstart_{parent} - dx_{child} \times add_w \quad (9)$$

$$start_x = \frac{X_{min} - xstart_{parent}}{dx_{par}} \quad (10)$$

### 2.2 Sub-grid nearest method in Downscale

Intersect and nearest methods are commonly used to downscale REI into user-defined domains. The intersect method obtains overlapping areas between the REI and the target domain, while the nearest method assigns emissions based on the nearest REI value. The intersect method accurately reflects the spatial relationship between the target domain and the REI. However, if there are evident projection and spatial resolution differences between REI and the target domain, a large number of small intersections are created, which significantly decreases calculation efficiency. The nearest method addresses this limitation but may lead to emission mismatches due to spatial differences. For example, the nearest method ignored the orange grid emissions but exaggerated the contribution of the yellow grids in the research domain,

as shown in Fig. 3. To fully consider the advantages and disadvantages of these two algorithms, we used the sub-grid nearest method to allocate the emission inventory, as shown in Eqs. (11)–(13). Figure 3 depicts the process we used to obtain the REI values using the nearest and sub-grid nearest methods. The colors in the figure represent the REI values, and the symbols (such as \*) represent the grid ID. First, we introduced a “sub-grid ratio” to divide each grid into  $p$  sub-grids, such as nine sub-grids in each grid. Second, we adopted the conventional nearest method to locate the nearest REI values for each sub-grid. Third, we calculated the emissions for each sub-grid based on the nearest REI value and spatial surrogates. Finally, we obtained the emissions for each grid based on a summary of the sub-grid emissions in each grid. It should be ensured that  $SA_{region,I_{i,j,p}}$  is larger or equal to the sum of  $SA_{target,i,j,p}$  in the same region grid  $I_{i,j,p}$  based on the principle of mass conservation. This module can downscale regional emission inventories in a user-friendly and easy-to-use way based on a default or user-defined proxy without external tools such as ArcGIS.

$$E_{target,i,j} = \sum_p E_{target,i,j,p} \quad (11)$$

$$E_{target,i,j,p} = E_{region,I_{i,j,p}} \times R_{region,I_{i,j,p}} \times \frac{SA_{target,i,j,p}}{SA_{region,I_{i,j,p}}} \quad (12)$$

$$I_{i,j,p} = \text{Nearest}(\text{Grid}_{target,i,j,p}, \text{Grid}_{region}), \quad (13)$$

where  $i$  and  $j$  are the column and row number of the target grid,  $p$  is the sub-grid ID in grid  $(i, j)$ ,  $E_{target,i,j}$  is the emissions in grid  $(i, j)$ ,  $E_{target,i,j,p}$  is the emissions in sub-grid  $p$  in grid  $(i, j)$ ,  $I_{i,j,p}$  is the location of sub-grid  $p$  for the target grid  $(i, j)$  in the region domain,  $E_{region,I_{i,j,p}}$  represents the regional emissions in  $I_{i,j,p}$ ,  $SA_{region,I_{i,j,p}}$  is the spatial allocator for region grid  $I_{i,j,p}$ ,  $SA_{target,i,j,p}$  is the spatial allocator for sub-grid  $p$  of target grid  $(i, j)$ ,  $\text{Grid}_{region}$  is the domain of the REI, and  $\text{Grid}_{target,i,j,p}$  is the sub-grid  $p$  of target grid  $(i, j)$ ;  $R_{region,I_{i,j,p}}$  is an adjustment factor to ensure mass conservation.

### 2.3 User-friendly emission source sector ID in Prepmoel

User-friendly emission source sector IDs (EIDs) are source abbreviations: for example, AG for agriculture. The EID is a unique ID for the emission source sector in ISAT. Speciate and temporal profiles for sectors can be easily defined with an EID, as shown in Table 1, where the speciate profile and point emission inventory are prefixed by `Speciate_` and `STACK_GROUP_` and suffixed by an EID. The area emission inventory was called EID. To define a temporal profile for each sector, users can add columns labeled by EID in `hourly.csv`, `weekly.csv`, and `monthly.csv`, as shown in Table 2. Users can easily add or delete sources in a model-ready emission inventory according to their needs in Prepmoel.

**Table 1.** File structure defined by emission source sector ID (EID).

File type	Filename	Example
Speciate profile	Speciate_\$(EID).csv	Speciate_IN.csv; Speciate_PP.csv; Speciate_AG.csv; Speciate_AR.csv
Area emission	\$(EID).csv	AR.csv; AG.csv
Point emission	STACK_GROUP_\$(EID).csv	STACK_GROUP_IN.csv; STACK_GROUP_PP.csv

**Table 2.** Case of temporal profiles (for PP source).

hourly.csv	weekly.csv		monthly.csv		
Hourly*	PP	Weekly	PP	Monthly	PP
0	0.045	0	0.145	1	0.090
1	0.047	1	0.144	2	0.065
2	0.046	2	0.143	3	0.083
3	0.045	3	0.144	4	0.075
4	0.043	4	0.143	5	0.075
...	...	5	0.138	...	...
23	0.044	6	0.143	12	0.098

\* UTC.

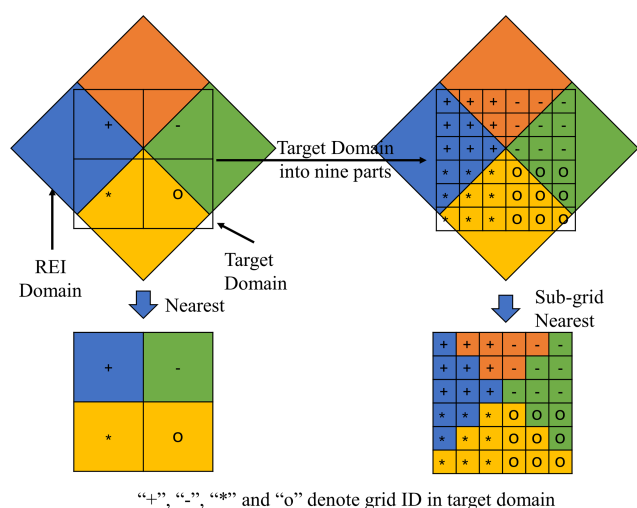


**Figure 3.** Concept of the sub-grid nearest method.

## 2.4 User-friendly speciation profile structure in Prepmodel

Compared with multiple input file types for chemical speciation in the SMOKE model, including GSCNV, GSPRO, GSPRODESC, GSPRO\_COMBO, GSREF, and GSTAG files, this tool simplifies the process with individual speciate profiles for each sector. An example of a speciate profile is shown in Table 3. Here, “pollutant” denotes the pollutants in the emission inventory, “species” denotes the pollutants in the chemical mechanism adopted in the AQM,

“split\_factor” represents the fraction of the pollutant emission to species in the AQM between zero and 1 (and it must be mass-conservative), “unit” is the unit of species adopted in the AQM (such as “moles/s” for gaseous pollutants and “g/s” for particulate pollutants), and “divisor” converts mass-based speciation into mole-based speciation, with molar mass for gaseous pollutants and a default value (set to 1) for particulate pollutants. Therefore, the user can easily modify the speciation profile based on the chemical mechanism in the AQM and the pollutants in the emission inventory.

In addition, we embedded a gridded spatial surrogate for roads and populations in the ISAT. The road database was obtained from OpenStreetMap, with four levels, including motorway, secondary road, primary road, and residential road. The standard road length (Zheng et al., 2009), based on vehicle speed, number of lanes, and road width from the Code for Transport Planning on Urban Roads (GB 50220-95) in China, was used to calculate the gridded road map data. Population density data based on the 2020 LandScan Global Population Database (Rose et al., 2021) can be used in ISAT with NetCDF. Users can also prepare any proxy for their needs. For example, land use and point of interest (POI) data are recommended for agriculture and residential sectors (Wang et al., 2017; Huang et al., 2022). Due to the nearly 1 km resolution of the ISAT-embedded gridded population and road maps, users can generate HREIs with finer spatial resolution  $> 1$  km.

**Table 3.** Case of speciate profile in ISAT.

Pollutant	Species	split_factor	Divisor	Unit	Pollutant	Species	split_factor	Divisor	Unit
CB05_ALD2	ALD2	1.00	44	mole s <sup>-1</sup>	PM <sub>2.5</sub>	PH <sub>2</sub> O	0.00	1	g s <sup>-1</sup>
CB05_ALDX	ALDX	1.00	45	mole s <sup>-1</sup>	PM <sub>2.5</sub>	PK	0.00	1	g s <sup>-1</sup>
CB05_ETH	ETH	1.00	28	mole s <sup>-1</sup>	PM <sub>2.5</sub>	PMG	0.00	1	g s <sup>-1</sup>
CB05_ETHA	ETHA	1.00	30	mole s <sup>-1</sup>	PM <sub>2.5</sub>	PMN	0.00	1	g s <sup>-1</sup>
CB05_ETOH	ETOH	1.00	46	mole s <sup>-1</sup>	PM <sub>2.5</sub>	PMOTHR	0.06	1	g s <sup>-1</sup>
CB05_FORM	FORM	1.00	30	mole s <sup>-1</sup>	PM <sub>2.5</sub>	PNA	0.00	1	g s <sup>-1</sup>
CB05_IOLE	IOLE	1.00	55	mole s <sup>-1</sup>	PM <sub>2.5</sub>	PNCOM	0.10	1	g s <sup>-1</sup>
CB05_ISOP	ISOP	1.00	68	mole s <sup>-1</sup>	PM <sub>2.5</sub>	PNH <sub>4</sub>	0.01	1	g s <sup>-1</sup>
CB05_MEOH	MEOH	1.00	32	mole s <sup>-1</sup>	PM <sub>2.5</sub>	PNO <sub>3</sub>	0.00	1	g s <sup>-1</sup>
CB05_NVOL	NVOL	1.00	1	mole s <sup>-1</sup>	PM <sub>2.5</sub>	POC	0.63	1	g s <sup>-1</sup>
CB05_OLE	OLE	1.00	30	mole s <sup>-1</sup>	PM <sub>2.5</sub>	PSI	0.00	1	g s <sup>-1</sup>
CB05_PAR	PAR	1.00	17	mole s <sup>-1</sup>	PM <sub>2.5</sub>	PSO <sub>4</sub>	0.01	1	g s <sup>-1</sup>
CB05_TERP	TERP	1.00	136	mole s <sup>-1</sup>	PM <sub>2.5</sub>	PTI	0.00	1	g s <sup>-1</sup>
CB05_TOL	TOL	1.00	101	mole s <sup>-1</sup>	SO <sub>2</sub>	SO <sub>2</sub>	1.00	64	mole s <sup>-1</sup>
CB05_UNR	UNR	1.00	19	mole s <sup>-1</sup>	SO <sub>2</sub>	SULF	0.01	98	mole s <sup>-1</sup>
CB05_XYL	XYL	1.00	114	mole s <sup>-1</sup>	NH <sub>3</sub>	NH <sub>3</sub>	1.00	17	mole s <sup>-1</sup>
PM <sub>2.5</sub>	PAL	0.00	1	g s <sup>-1</sup>	CO	CO	1.00	28	mole s <sup>-1</sup>
PM <sub>2.5</sub>	PCA	0.00	1	g s <sup>-1</sup>	PMcoarse	PMC	1.00	1	g s <sup>-1</sup>
PM <sub>2.5</sub>	PCL	0.00	1	g s <sup>-1</sup>	NO <sub>x</sub>	NO	0.90	30	mole s <sup>-1</sup>
PM <sub>2.5</sub>	PEC	0.18	1	g s <sup>-1</sup>	NO <sub>x</sub>	NO <sub>2</sub>	0.09	46	mole s <sup>-1</sup>
PM <sub>2.5</sub>	PFE	0.00	1	g s <sup>-1</sup>					

### 3 Case studies

As the capital of China, Beijing has a large population and number of vehicles, making it a hotspot for air pollution research in China (Gao et al., 2018; X. Huang et al., 2021). This study presents three nested-domain cases: mainland China, Beijing–Tianjin–Hebei (BTH), and Beijing (BJ), with spatial resolutions of 27, 9, and 3 km, respectively, as shown in Fig. 4. The ISAT was used for the workflow from the nested-domain configuration to the model-ready inventory for the WRF-AQM. The shapefile for these domains was used to configure nested domains in the WRF-AQM and to create the ready emission inventory in the Prepgrid module. Provincial pollutant sources in transportation and residential sectors in Beijing (BMEE, 2021) were allocated into 3 km × 3 km grids by the Mapinv module. The MEIC regional emission inventory with a spatial resolution of 0.25° × 0.25° in 2020 was downscaled to grid level in the Downscale module.

#### 3.1 Nested-domain configuration by Prepgrid

ISAT provides comprehensive grid information for the WRF-AQM in comma-separated value (.csv) files and shapefile formats. Data formatted in .csv contain grid information for each domain and can be further used as the input for other ISAT modules. Shapefile-formatted data can be displayed directly in ArcGIS or other geographic information system to display and check the configuration for nested domains. “Domainname” and “Casename” were used to mark the

**Figure 4.** The three nested domains and their shapefiles.

output in the Prepgrid module. “\${Casename}\_gridinfo.csv” summarizes grid information in nested domains and can be used to configure domain parameters in the WRF model, as shown in Fig. 5b. “wrf\_\${Domainname}.shp” and “wrf\_\${Domainname}.csv” provided shapefile and grid information for the ISAT-configured WRF model. “aqm\_\${Domainname}.shp” and



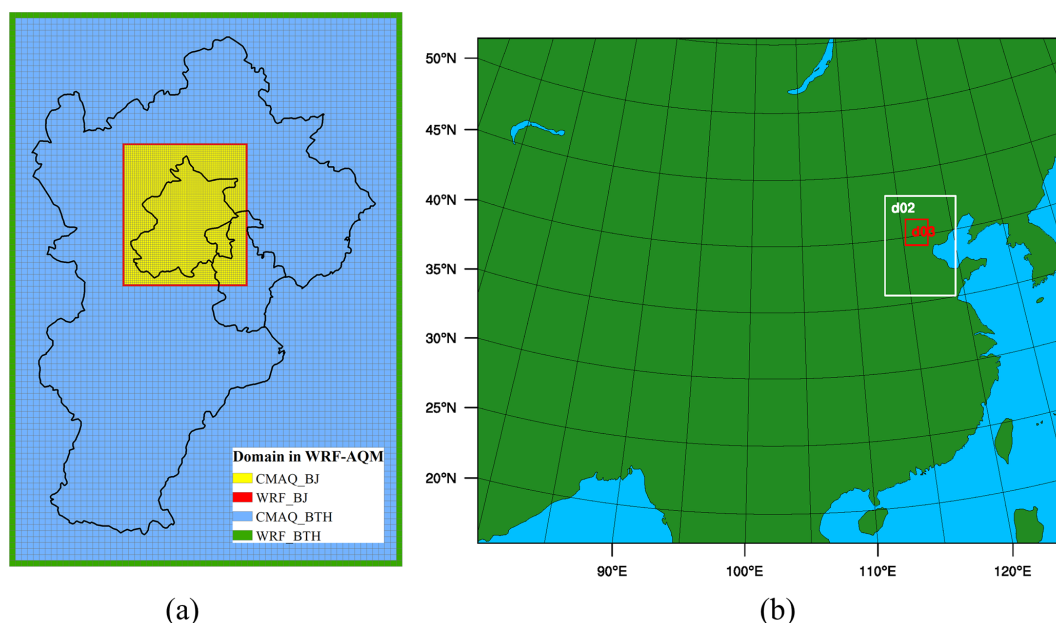


**Figure 5.** ISAT-configured WRF-AQM nested domains.

“aqm\_{\$Domainname}.csv” were the shapefile and grid information for the ISAT-configured AQM. Due to the blend of larger-scale driving data and scale-specific physics, the outermost cells in the WRF domain are inappropriate to use and usually removed in AQM (US EPA, 2019). The ISAT-configured domains reflect this requirement of a lateral boundary in AQM and accurately obtain the WRF-AQM domain.

### 3.2 Downscaled regional emissions inventory by Downscale

The MEIC inventory is widely used in China. In this study, the 2020 annual MEIC emissions were preprocessed into .csv format and downscaled into the AQM domain by the Downscale module. Compared with ArcGIS, SMOKE, and other tools, using the Downscale module reduces the timeliness from hours to minutes. We compared gridded residential emissions in BTH under different downscaled method, including the intersect method, nearest method, and sub-grid nearest method. The sub-grid ratio, the key parameter in the sub-grid nearest method, must either be 1 or a multiple of 3 and applied to test the allocation result. Therein, the nearest method can be configured with a sub-grid ratio equal to 1. With the sub-grid ratio increased from 1 to 9, the spatial allocation was close to the result of the intersect method for the urban area, as shown in Fig. 6. The sub-grid method with a sub-grid ratio equal to 3 significantly improved the allocation compared to the nearest method, and the *R*-squared increased from 0.91 to 0.98. The increase in the sub-grid ratio from 3 to 9 slightly improved the distribution results, with *R*-squared increasing from 0.979 to 0.984, as shown in Fig. 7. Although

a higher sub-grid ratio may lead to a more accurate allocation, one needs to consider the computational efficiency and resolution of the spatial surrogate. For example, the running time of the “downscaled” module increased from 2 to 10 min, and the sub-grid ratio increased from 3 to 9 in this case. In addition, for REI grids with empty spatial surrogates, ISAT applies the grid area as a weight when allocating emissions. Constrained by the spatial surrogate ( $\leq 1$ ) for each REI grid based on the principle of mass conservation, the downscaled emission inventory exhibited good agreement with the REI. Regarding the result of the intersect method as the true value, the relative error of total PM<sub>2.5</sub> emissions under each sub-grid ratio is less than 0.2 %, which reflects the good quality of the downscaling in terms of mass flux conservation.

These downscaled REIs can be used to produce model-ready emissions for domains without a local emission inventory. Due to more detailed and realistic emission characteristics, a local emission inventory is highly recommended based on spatial–temporal emission characteristic research and simulation in WRF-AQM in the innermost domain.

### 3.3 Gridded local emission inventory by Mapinv

Differing from the downscale process used for the gridded REI described in Sect. 3.2, mapping the provincial- and/or city-level local emission inventory onto the grid level required the identification of region attributes for each AQM domain and the allocation of emissions based on spatial surrogates. In ISAT v2.0, users can add a column to define the region in the shapefile and input the local emission inventory in the “localinv” file. ISAT will allocate the local emission inventory for each species to grid level. Taking Beijing as

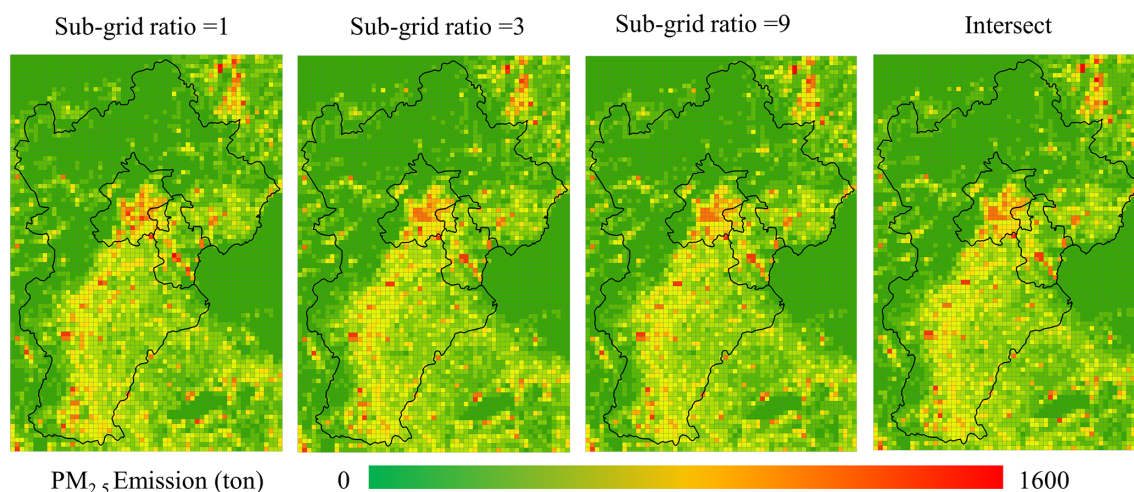


**Figure 6.** Comparison of the intersect and the sub-grid nearest method allocations with different sub-grid ratios.

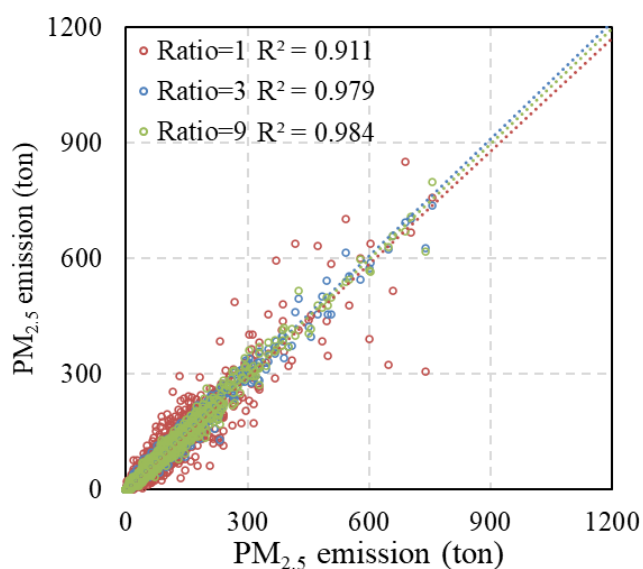


**Figure 7.** Pairwise relationship between the intersect and sub-grid nearest methods with different sub-grid ratios for particulate matter (PM).

an example, emissions for the occupied residential (RE) and transportation sectors were 7763 t NO<sub>x</sub> with 25 900 t VOCs and 22 700 t NO<sub>x</sub> with 2654 t VOCs, respectively. The gridded emission inventory for the occupied residential (RE) and transportation (TR) sectors created by the ISAT reflected the spatial variations in population density and the road map in Beijing, as shown in Fig. 8. Based on the embedded population density and road map, ISAT could flexibly allocate the local emission inventory to grid level.

### 3.4 Model-ready emission inventory by Prepmode

Users can generate inline-format model-ready emission inventories for AQM using the Prepmode module. The gridded emission inventory generated by Mapinv and Downscale can be used as area emission input files. The point emission file was organized into .csv format, which contained emissions, locations, and stack parameters with reference to the SMOKE model. Temporal profile files were defined based on statistical data and previous studies. The speciation profiles for sectors were obtained from the SPECIATE database or field measurements. Moreover, GRIDCRO2D files generated by the Meteorology–Chemistry Interface Processor in the CMAQ model were applied to provide global attributes and configurations consistent with the AQM. “Runtime” was used to define the model-ready emission time steps for the AQM. The ISAT inline-format emission inventory was named EID. For example, “TR.nc” denoted the area emission source for the TR sector. “PPpoint.nc” and “STACK\_GROUP\_PP.nc” represented hourly emissions and the source information for the power plants, respectively. The model-ready emission inventory can be directly used in AQMs, such as CMAQ and CAMx, as well as instrumental modules, such as the decoupled direct method (DDM) and integrated source apportionment method (ISAM). Previous studies achieved reliable simulation results using this approach (H. Wang et al., 2021; K. Wang et al., 2022a, 2021a, b; Liu et al., 2023; Li, 2021; Tan, 2022).

The configurations and steps used in these cases are detailed in Appendix A.

## 4 Conclusion

We have developed an integrated tool, ISAT v2.0, that streamlines the workflow from a nested-domain configura-



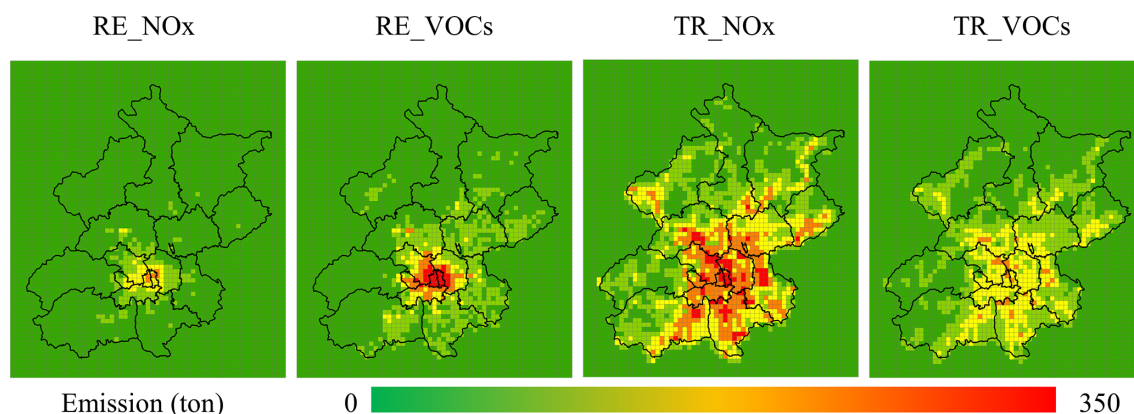


**Figure 8.** Spatial allocation for Beijing.

tion to a model-ready emission inventory for WRF-AQM. ISAT v2.0 consists of four main modules: Prepgrid, Downscale, Mapinv, and Prepmodel. The Prepgrid module can accurately provide user-defined domain configuration under nesting rules in WRF-AQM and the shapefile of the study area. It can also configure the namelist.wps file in WPS using domain parameters defined in this module. The Downscale module conducted with the “sub-grid nearest” method significantly improved the allocation result in comparison to the Downscale module with the nearest method. Moreover, users can flexibly set the “sub-grid ratio” according to their specific needs. The Mapinv module provides a user-friendly tool to allocate a provincial- and/or city-level local emission inventory to grid level using user-defined shapefiles and local emission inventories. Finally, the Prepmodel module can generate an inline-format model-ready file emission inventory for WRF-AQM and provides users with the numerical simulations. ISAT is free, expandable, and supported by both Linux and Windows, and it can be applied to process other regional emission inventories, such as REAS, by providing grid templates and updating user-defined spatial surrogates. Relying on the established relationship between the shapefile and the WRF-AQM domain, ISAT is highly extendable, including the creation of ocean files in CMAQ models (US EPA, 2019), the labeling of source regions in CAMX-PSAT, and other potential uses.

## Appendix A: ISAT step-by-step guide

Taking the nested domains in Fig. 4 with a spatial resolution of “27km-9km-3km” as an example.

### Step 1: obtain nested-domain parameters for WRF-AQM based on the domain shapefile

#### (a) Give the information of “par.ini” in the Prepgrid module

lat1:33.0	# First standard latitude for LCC
lat2:42.0	# Second standard latitude for LCC
casename:3nestdomain	# Case name
numdom:3	# Number of nested domains
shpath: ./shp/mainlandchina.shp, ./shp/JJJ.shp, ./shp/beijing.shp	# Shpfile path for domains
dx:27000,9000,3000	# Resolution in meters for domains
xladd:2,3,3	# Added grid in left in x direction
xradd:2,3,3	# Added grid in right in x direction
ytadd:2,3,3	# Added grid in top in y direction
ydadd:2,3,3	# Added grid in down in y direction
domainname:MainlandChina,JJJ,Beijing	# Name for domains
model_clip:1,1,1	# Clip number of grids for AQM

#### (b) Running the Prepgrid module by “python prepgrid.py” – domain information summarized in “3nestdomain\_gridinfo.csv”, detailed below

domid	centlon	centlat	xmin	ymin	numx	numy	xstart	ystart
0	102.0737	36.68731	−2 484 000	−2 119 500	184	157	0	0
1	102.0737	36.68731	945 000	−40 500	66	93	127	77
2	102.0737	36.68731	1 116 000	382 500	63	72	19	47

Therein, you can define the WPS domain the using variables above

parent_id	1	1	2
parent_grid_ratio	1	3	3
i_parent_start	1	\$xstart(1) + 1	\$xstart(2) + 1
j_parent_start	1	\$ystart(1) + 1	\$ystart(2) + 1
e_we	\$numx(0) + 1	\$numx(1) + 1	\$numx(2) + 1
e_sn	\$numy(0) + 1	\$numy(1) + 1	\$numy(2) + 1
ref_lat	\$centlat		
ref_lon	\$centlon		
truelat1	\$lat1		
stand_lon	\$centlon		
truelat2	\$lat2		

#### (c) You can get a fishnet shapefile for the WRF model called “wrf\_” + \${domainname} + “.shp” and AQM called “aqm\_” + \$domainname + “.shp”

#### (d) You can also get gridded information for domains in “wrf\_” + \${domainname} + “.csv” for the WRF model and “aqm\_” + \$domainname + “.shp” for AQM, respectively

## Step 2: downscaling regional emission inventory into target domains

### (a) Give the information of “par.ini” in the Downscale module

```

invf:./input/domain/aqmJJJ.csv      # Path of target domain information
dx:9000                             # Resolution in meters for target domain
ratio:3                             # Sub-grid ratio
emissions: ./regioninv/agricultureannual.csv,./regioninv/
regioninv/transportationannual.csv,./regioninv/
residentialannual.csv              # Path for regional emission inventory
casename:JJJ                       # Case name
method:area,road,pop               # Allocation method for specific emission inventory
area: based on grid area
road: based on roads map
pop: based on population map

```

### (b) Running the Downscale module by “python downscale.py” and getting gridded emissions for specific area sources

## Step 3: preparation of model-ready emission inventories for AQM

### (a) Give the information of “par.ini” in the Prepmodel module

```

runtime:193                         # Time steps for AQM run
gridcro2d: ./src/met/GRIDCRO2D_9km  # MCIP generated GRIDCRO2D file
speciate: ./src/speciate/speciate_AR.csv, ./src/speciate/speciate_AG.csv # Speciation profile for area emission sources.
speciate_groups: ./src/speciate/speciate_IN.csv # Speciation profile for point emission sources.
temporary_hour : ./src/temporary/hourly.csv # Hourly temporal profile for emission sources.
temporary_week : ./src/temporary/weekly.csv # Weekly temporal profile for emission sources.
temporary_month: ./src/temporary/monthly.csv # Monthly temporal profile for emission sources.
emissions: ./src/emissions/MEIC/AR.csv, ./src/emissions/MEIC/AG.csv # Path of area emission files
stack_groups: ./src/emissions/MEIC/STACK_GROUP_IN.csv # Path of point emission files

```

### (b) Run the Prepmodel module by “python area\_emis.py; python point\_emis.py; python point\_info.py” – for the CAMx model, CMAQ2CAMx can be used transfer this output into CAMx

## Other step: mapping a local emission inventory to the grid level

### (a) Give the information of “par.ini” in the Mapinv module

```

regionshp:./input/Region/BJ.shp    # Shapefile for region
Key:NAME                           # Region column in shapefile
grid:./input/Grid/3km.csv          # Grid information by “pregrid”
sapath:./input/SA/inv_sa_tmp_road.csv,./input/SA/inv_sa_tmp_pop.csv # Spatil surrogated by “downscale” module
localinv:./input/localinv/TR.csv,./input/localinv/RE.csv # Path way for local emission inventory
localname:TR3KM,AR3KM              # Name of gridded emission inventory output

```

### (b) Run the Mapinv module by “python mapinv.py”

**Code and data availability.** The source code of ISAT v2.0 and input data used to produce the results used in this paper are archived on Zenodo at <https://doi.org/10.5281/zenodo.7481439> (Wang et al., 2022b).

**Author contributions.** KuW: conceptualization, methodology, software, writing – original draft; CG, KaW, HW, and QT: data curation; MD: writing – review and editing; KL and XJ: resources, supervision, investigation.

**Competing interests.** The contact author has declared that none of the authors has any competing interests.

**Disclaimer.** Publisher's note: Copernicus Publications remains neutral with regard to jurisdictional claims in published maps and institutional affiliations.

**Acknowledgements.** The authors are very grateful to Xuelei Zhang, Wenbo Xue, Shuhan Liu, and Xin Bo for providing guidance on developing ISAT.

**Financial support.** This research has been supported by the National Key Research and Development Program of China (grant no. 2019YFE0194500), the European Union's Horizon 2020 Research and Innovation program under grant agreement no. 870301 (AQ-WATCH), and BJASt Scientific Research in 2022 (grant no. 11000022T000000468154).

**Review statement.** This paper was edited by Yilong Wang and reviewed by two anonymous referees.

## References

- Baek, B. and Seppanen, C.: CEMPD/SMOKE: SMOKE v4.8.1, Zenodo [code], <https://doi.org/10.5281/ZENODO.4480334>, 2021.
- Beijing Municipal Ecology and Environment Bureau (BMEE): Second National Pollution Source Census Bulletin in Beijing, 2021.
- Burnett, R., Chen, H., Szyszkowicz, M., Fann, N., Hubbell, B., Pope, C., Apte, J., Brauer, M., Cohen, A., Weichenthal, S., Cogging, J., Di, Q., Brunekreef, B., Frostad, J., Lim, S., Kan, H., Walker, K., Thurston, G., Hayes, R., Lim, C., Turner, M., Jerrett, M., Krewski, D., Gapstur, S., Diver, R., Ostro, B., Goldberg, D., Crouse, D., Martin, R., Peters, P., Pinault, L., Tjepkema, M., van Donkelaar, A., Villeneuve, P., Miller, A., Yin, P., Zhou, M., Wang, L., Janssen, N., Marra, M., Atkinson, R., Tsang, H., Quoc, T., Cannon, J., Allen, R., Hart, J., Laden, F., Cesaroni, G., Forastiere, F., Weinmayr, G., Jaensch, A., Nagel, G., Concin, H., and Spadaro, J.: Global estimates of mortality associated with long-term exposure to outdoor fine particulate matter, *P. Natl. Acad. Sci. USA*, 115, 9592–9597, <https://doi.org/10.1073/pnas.1803222115>, 2018.
- Daniels, M., Lundquist, K., Mirocha, J., Wiersema, D., and Chow, F.: A New Vertical Grid Nesting Capability in the Weather Research and Forecasting (WRF) Model, *Mon. Weather Rev.*, 144, 3725–3747, 2016.
- European Commission Joint Research Centre (ECJRC): Downscaling methodology to produce a high-resolution gridded emission inventory to support local/city level air quality policies, Publications Office, LU, <https://doi.org/10.2760/51058>, 2017.
- Eyth, A. and Hanisak, K.: The MIMS Spatial Allocator: A Tool for Generating Emission Surrogates without a Geographic Information System, <https://www3.epa.gov/ttnchie1/conference/ei12/modeling/eyth.pdf> (last access: 30 March 2023), 2003.
- Gao, J., Wang, K., Wang, Y., Liu, S., Zhu, C., Hao, J., Liu, H., Hua, S., and Tian, H.: Temporal-spatial characteristics and source apportionment of PM<sub>2.5</sub> as well as its associated chemical species in the Beijing-Tianjin-Hebei region of China, *Environ. Pollut.*, 233, 714–724, <https://doi.org/10.1016/j.envpol.2017.10.123>, 2018.
- Guevara, M., Soret, A., Arévalo, G., Martínez, F., and Baldasano, J.: Implementation of plume rise and its impacts on emissions and air quality modelling, *Atmos. Environ.*, 99, 618–29, 2014.
- Huang, C., Wang, H. L., Li, L., Wang, Q., Lu, Q., de Gouw, J. A., Zhou, M., Jing, S. A., Lu, J., and Chen, C. H.: VOC species and emission inventory from vehicles and their SOA formation potentials estimation in Shanghai, China, *Atmos. Chem. Phys.*, 15, 11081–11096, <https://doi.org/10.5194/acp-15-11081-2015>, 2015.
- Huang, C., Zhuang, Q., Meng, X., Zhu, P., Han, J., and Huang, L.: A fine spatial resolution modelling of urban carbon emissions: a case study of Shanghai, China, *Sci. Rep.*, 12, 9255, <https://doi.org/10.1038/s41598-022-13487-5>, 2022.
- Huang, X., Tang, G., Zhang, J., Liu, B., Liu, C., Zhang, J., Cong, L., Cheng, M., Yan, G., Gao, W., Wang, Y., and Wang, Y.: Characteristics of PM<sub>2.5</sub> pollution in Beijing after the improvement of air quality, *J. Environ. Sci.*, 100, 1–10, <https://doi.org/10.1016/j.jes.2020.06.004>, 2021.
- Huang, Z., Zhong, Z., Sha, Q., Xu, Y., Zhang, Z., Wu, L., Wang, Y., Zhang, L., Cui, X., Tang, M., Shi, B., Zheng, C., Zhen, L., Hu, M., Bi, L., Zheng, J., and Yan, M.: An updated model-ready emission inventory for Guangdong Province by incorporating big data and mapping onto multiple chemical mechanisms, *Sci. Total Environ.*, 769, 144535, <https://doi.org/10.1016/j.scitotenv.2020.144535>, 2021.
- Li, M., Liu, H., Geng, G., Hong, C., Liu, F., Song, Y., Tong, D., Zheng, B., Cui, H., Man, H., Zhang, Q., and He, K.: Anthropogenic emission inventories in China: a review, *Natl. Sci. Rev.*, 4, 834–866, <https://doi.org/10.1093/nsr/nwx150>, 2017.
- Li, Y.: Study on Ozone Formation Sensitivity in the Pearl River Delta based on Satellite Remote Sensing and Air quality Model, Master's Thesis, South China University of Technology, <https://doi.org/10.27151/d.cnki.ghnlu.2021.005599>, 2021.
- Lin, P., Gao, J., Xu, Y., Schauer, J., Wang, J., He, W., and Nie, L.: Enhanced commercial cooking inventories from the city scale through normalized emission factor dataset and big data, *Environ. Pollut.*, 315, 120320, <https://doi.org/10.1016/j.envpol.2022.120320>, 2022.

- Liu S., Liu, K., Wang, K., Chen, X., and Wu, K.: Fossil-Fuel and Food Systems Equally Dominate Anthropogenic Methane Emissions in China, *Environ. Sci. Technol.*, 2023, 57, 6, 2495–2505, <https://doi.org/10.1021/acs.est.2c07933>, 2023.
- Monforti, F. and Pederzoli, A.: THOSCANE: a tool to detail CORINAIR emission inventories, *Environ. Modell. Softw.*, 20, 505–508, <https://doi.org/10.1016/j.envsoft.2004.07.001>, 2005.
- Namdeo, A., Mitchell, G., and Dixon, R.: TEMMS: an integrated package for modelling and mapping urban traffic emissions and air quality, *Environ. Modell. Softw.*, 17, 177–188, [https://doi.org/10.1016/S1364-8152\(01\)00063-9](https://doi.org/10.1016/S1364-8152(01)00063-9), 2002.
- Rose, A., McKee, J., Sims, K., Edward, B., Andrew, R., and Marie, U.: LandScan Global 2020, Oak Ridge National Laboratory [data set], <https://doi.org/10.48690/1523378>, 2021.
- Skamarock, W. C., Klemp, J. B., Dudhia, J., Gill, D., Liu, Z., Berner, J., Wang, W., Powers, J., Duda, M., Barker, D., and Huang, X.: A Description of the Advanced Research WRF Model Version 4, UCAR/NCAR, <https://doi.org/10.5065/1DFH-6P97>, 2019.
- Tan, X.: Construction of CMAQ Pollution Source Inventory Based on ISAT Model, Master's Thesis, Jilin University, <https://doi.org/10.27162/d.cnki.gjlin.2022.003751>, 2022.
- United States Environmental Protection Agency (US EPA): CMAQ User's Guide, GitHub, [https://github.com/USEPA/CMAQ/blob/main/DOCS/Users\\_Guide](https://github.com/USEPA/CMAQ/blob/main/DOCS/Users_Guide) (last access: 30 March 2023), 2019.
- Wang, H., Liu, Z., Zhang, Y., Yu, Z., and Chen, C.: Impact of different urban canopy models on air quality simulation in Chengdu, southwestern China, *Atmos. Environ.*, 267, 118775, <https://doi.org/10.1016/j.atmosenv.2021.118775>, 2021.
- Wang, H., Liu, Z., Wu, K., Qiu, J., Zhang, Y., Ye, B., and He, M.: Impact of Urbanization on Meteorology and Air Quality in Chengdu, a Basin City of Southwestern China, *Front. Ecol. Evol.*, 10, 845801, <https://doi.org/10.3389/fevo.2022.845801>, 2022.
- Wang, K., Gao, J., Tian, H., Dan, M., Yue, T., Xue, Y., Zuo, P., and Wang, C.: An emission inventory spatial allocate method based on POI data, *China Environmental Science*, 37, 2377–2382, 2017.
- Wang, K., Tong, Y., Yue, T., Gao, J., Wang, C., Zuo, P., and Liu, J.: Measure-specific environmental benefits of air pollution control for coal-fired industrial boilers in China from 2015 to 2017, *Environ. Pollut.*, 273, 116470, <https://doi.org/10.1016/j.envpol.2021.116470>, 2021a.
- Wang, K., Tong, Y., Gao, J., Zhang, X., Zuo, P., Wang, C., Wu, K., and Yang, S.: Pinpointing optimized air quality model performance over the Beijing-Tianjin-Hebei region: Mosaic approach, *Atmos. Pollut. Res.*, 12, 101207, <https://doi.org/10.1016/j.apr.2021.101207>, 2021b.
- Wang, K., Gao, J., Liu, K., Tong, Y., Dan, M., Zhang, X., and Liu, C.: Unit-based emissions and environmental impacts of industrial condensable particulate matter in China in 2020, *Chemosphere*, 303, 134759, <https://doi.org/10.1016/j.chemosphere.2022.134759>, 2022a.
- Wang, K., Gao, C., Wang, H., Wu, K., Tong, Q., Mo, D., Ji, X., and Liu, K.: Inventory Spatial Allocate Tool v2.0 source code, Zenodo [code and data set], <https://doi.org/10.5281/zenodo.7481439>, 2022b.
- Zhang, X., Gurney, K. R., Rayner, P., Liu, Y., and Asefi-Najafabady, S.: Sensitivity of simulated CO<sub>2</sub> concentration to regridding of global fossil fuel CO<sub>2</sub> emissions, *Geosci. Model Dev.*, 7, 2867–2874, <https://doi.org/10.5194/gmd-7-2867-2014>, 2014.
- Zheng, B., Tong, D., Li, M., Liu, F., Hong, C., Geng, G., Li, H., Li, X., Peng, L., Qi, J., Yan, L., Zhang, Y., Zhao, H., Zheng, Y., He, K., and Zhang, Q.: Trends in China's anthropogenic emissions since 2010 as the consequence of clean air actions, *Atmos. Chem. Phys.*, 18, 14095–14111, <https://doi.org/10.5194/acp-18-14095-2018>, 2018.
- Zheng, B., Cheng, J., Geng, G., Wang, X., Li, M., Shi, Q., Qi, J., Lei, Y., Zhang, Q., and He, K.: Mapping anthropogenic emissions in China at 1 km spatial resolution and its application in air quality modeling, *Science Bulletin*, 66, 612–620, <https://doi.org/10.1016/j.scib.2020.12.008>, 2021.
- Zheng, J., Che, W., Wang, X., Louie, P., and Zhong, L.: Road-Network-Based Spatial Allocation of On-Road Mobile Source Emissions in the Pearl River Delta Region, China, and Comparisons with Population-Based Approach, *J. Air Waste Manage.*, 59, 1405–1416, <https://doi.org/10.3155/1047-3289.59.12.1405>, 2009.
- Zhou, Y., Zhao, Y., Mao, P., Zhang, Q., Zhang, J., Qiu, L., and Yang, Y.: Development of a high-resolution emission inventory and its evaluation and application through air quality modeling for Jiangsu Province, China, *Atmos. Chem. Phys.*, 17, 211–233, <https://doi.org/10.5194/acp-17-211-2017>, 2017.
- Zhuang, J., Dussin, R., Huard, D., Bourgault, P., Banihirwe, A., Raynaud, S., Malevich, B., Schupfner, M., Levang, S., Juling, A., Almansi, M., Filpe, RichardScot-tOZ., RondeauG., Rasp, S., Stachelek, J., Bell, R., Smith, T., and Li, X.: xESMF: v0.7.0 (v0.7.0), Zenodo [code], <https://doi.org/10.5281/zenodo.7447707>, 2022.